V European Conference on Computational Fluid Dynamics
ECCOMAS CFD 2010
J. C. F. Pereira and A. Sequeira (Eds)
Lisbon, Portugal, 14–17 June 2010

LARGE-EDDY SIMULATION OF THE AERODYNAMIC PITCHING STABILITY OF ROAD VEHICLE

Makoto Tsubokura[*], Seeyuan Cheng[*], Takuji Nakashima[†], Takahide Nouzawa[††] and Takaki Nakamura[††]

[*] Graduate School of Engineering, Hokkaido University
N13, W8, Kita-ku, Sapporo-shi, Hokkaido, 060-8628, Japan
e-mail: mtsubo@eng.hokudai.ac.jp

[†]Graduate School of Engineering, Hiroshima Unviersity
1-4-1 Kagamiyama, Higashi-Hiroshima-shi, Hiroshima, 739-8527, Japan
e-mail: nakashima@hiroshima-u.ac.jp

[††]Mazda Motor Corporation
3-1 Shinchi, Fuchu-cho, Aki-gun, Hiroshima, 730-8670Japan

Key words: Aerodynamics, Road Vehicle, Large-Eddy Simulation

Abstract. *Aerodynamic pitching stability of sedan-type road vehicle was investigated using the Large-Eddy Simulation technique. The study was based on two kinds of simplified vehicle models, which represent two real sedan-type vehicles with different pitching stability at on-road tests. The simplified vehicle modes were developed to reproduce the characteristic flow structures above the trunk deck of the real vehicles. Both models were seemingly identical and only the difference was their front and rear pillars shape. The aerodynamic pitching stability characteristics were determined through the phase-averaged pitching moment acting on both models by imposing the forced sinusoidal pitching oscillation as input. Arbitrary Lagrangian-Eulerian method was adopted to capture the dynamic motion of the models. It was demonstrated that the model representing the flow structures of the more stable sedan vehicle showed higher aerodynamic damping than the model of the less stable vehicle. It was concluded that pitching stability of sedan-type road vehicle is associated with the aerodynamic pitching damping mechanism caused by flow structures above the trunk deck, and the structures are strongly affected by slight geometrical difference of front and rear pillars.*

1 INTRODUCTION

In automotive industry, aerodynamic performances of road vehicle have been determined through averaged aerodynamic forces and moments acting on a vehicle subjected to steady incoming air. While in recent years, increasing attention has been paid to the effect of transient aerodynamics [1,2,3], which appears to be critical in the situations of such as gusty crosswind or overtaking. It is also assumed that ambient atmospheric turbulence around a vehicle in the real world more or less affects the averaged aerodynamic forces, and as a result, some discrepancies between the wind tunnel measurements and on-road conditions are observed.

In fact, it has been reported recently [4] that two sedan-type vehicles with almost the same aerodynamic drag and lift coefficients measured in a wind tunnel happened to show drastic difference of straight-ahead stability at on-road tests. It was discussed that flow structures above the trunk deck strongly affect the pitching motion of the vehicles, and suggested the importance of aerodynamic damping on the straight-ahead stability. They further investigated the difference of the flow structures between the two vehicles and realized that it was caused by the eddies generated at front and rear pillars.

In the succeeding report [5], they developed two simplified vehicle models which represent the two sedan-type vehicles investigated in the previous report in terms of the front and rear pillar shapes. Then, three dimensional flow structures above the trunk deck were extracted by Large-Eddy Simulation (LES) and validated through wind tunnel measurements. It was reported that the simplified models successfully reproduced the assumed flow structures of the real sedan vehicles. However, due to the low spatial resolution of LES in the dynamic pitching case, significant difference of aerodynamic damping factor between the two models and their mechanism caused by flow structures has not yet been reported.

Accordingly, the objective of this study is, based on the previous reports, to further investigate the aerodynamic damping effect between the two simplified vehicles with different pitching stability by using LES. In addition, an improved version of the model representing the higher pitching stability is introduced. The aerodynamic damping effect is estimated by imposing sinusoid pitching oscillation on the two vehicles, and the aerodynamic response of the forced oscillation is phase-averaged and decomposed into steady, quasi-steady, and dynamic components. The high performance computing LES with Arbitrary Lagrangian-Eulerian (ALE) technique specially designed for vehicle aerodynamics [6] is employed for the numerical simulation.

2 SIMPLIFIED SEDAN-TYPE VEHICLE MODELS

The 1:20 scale simplified vehicle model representing the sedan car of the unstable pitching as used by the previous study [5] is shown in Fig. 1a). The revised model from the previous one representing the stable pitching sedan is illustrated in Fig. 1b), which was developed to reproduce more intense rear-pillar vortices than the previous model. In addition, a more streamline profile is adopted near the trailing edge of the roof and a rib structure is introduced along the rear pillar. The models are of similar size, with length L, width W and height H measurements of 210, 80 and 65 mm, respectively. The main differences between the models that result in a totally different pitching stability characteristic appear at the front and rear pillar edges; Sharp-edged front pillar coupled with curved rear pillar for model represents the sedan car of lower pitching stability, and vice versa.

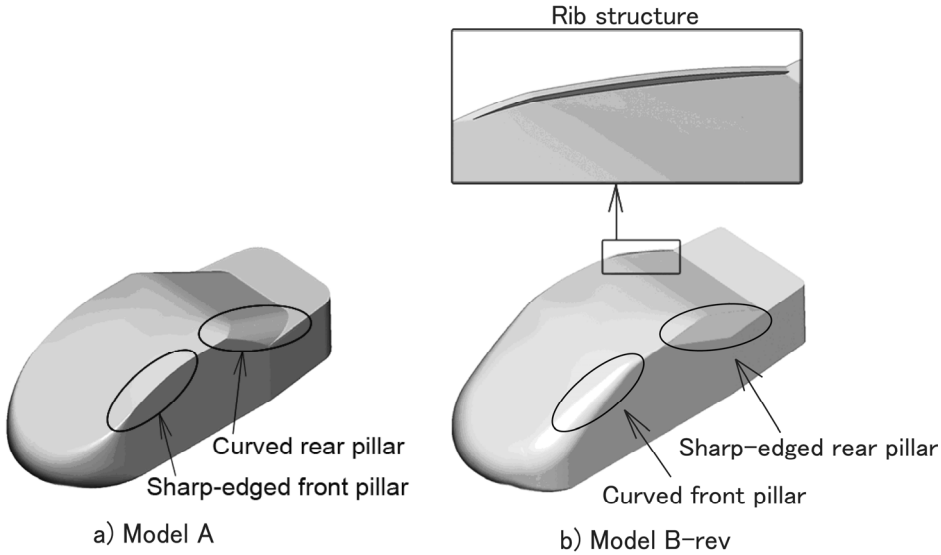

Figure 1: Simplified vehicle models.

3 NUMERICAL METHODS

3.1 Governing Equations

Incompressible and Newtonian fluid was assumed and the continuity and momentum equations were spatially filtered to obtain the governing equations of LES, which read as:

$$\frac{\partial \overline{u}_i}{\partial x_i} = 0 \quad , \tag{1}$$

$$\frac{\partial \overline{u}_i}{\partial t} + \frac{\partial \overline{u}_i \overline{u}_j}{\partial x_j} = -\frac{\partial \overline{P}}{\partial x_i} + 2\frac{\partial}{\partial x_j}(\nu + \nu_{sgs})\overline{S}_{ij} \quad , \tag{2}$$

in which u_i, ν, and ρ are the velocity for i direction, the kinetic viscosity, and fluid density, respectively. The bar over the physical quantity indicates the spatial filtering operation for LES. The filtered strain rate tensor $\overline{S}_{ij}$ and pressure $\overline{P}$ in eq. (2) are expressed as,

$$\overline{S}_{ij} = \frac{1}{2}\left(\frac{\partial \overline{u}_j}{\partial x_i} + \frac{\partial \overline{u}_i}{\partial x_j}\right) \quad , \tag{3}$$

$$\overline{P} = \overline{p}/\rho + (\overline{u_i u_j} - \overline{u}_i \overline{u}_j)/3 \quad . \tag{4}$$

In the eq. (2), the last term on the right represents the effect of subgrid-scale (SGS) turbulence, which is modeled under the eddy viscosity assumption. The conventional Smagorinsky's model[7] was adopted, and the eddy viscosity coefficient is modeled as

$$\nu_{sgs} = (C_s f \Delta)^2 \sqrt{2\overline{S}_{ij}\overline{S}_{ij}} \quad , \tag{5}$$

in which C_s is the model coefficient determined prior to the simulation, Δ is the length scale of the SGS turbulence and expressed as a cube root of each numerical mesh, and f represents the damping effect of SGS turbulence at the vicinity of the solid wall. The van Driest type damping function was adopted in the study, which is given as

$$f = 1 - \exp \frac{-l^+}{25}, \tag{6}$$

where l^+ is the distance from the solid wall in wall coordinate normalized by the surface friction and the kinetic viscosity. For the model parameter, Cs=0.15 was adopted in this study.

3.2 Discretization

The governing equations were discretized in space by a vertex-centered unstructured finite volume method. The second-order central differences were mainly applied for the spatial derivative, blended with the first-order upwind scheme for the convective term in the Navier-Stokes to avoid the excessive numerical oscillation appearing at coarse tetrahedral elements. It should be noted here that the dissipation property of upwind schemes is desirable to a certain extent for engineering applications of LES on unstructured meshes. As a compromise, the contribution of the upwind discretisation to the convective fluxes was set to be as low as 5%. The diffusive fluxes on the volume surface were treated based on the deferred correction formula suggested by Muzaferija[8] to avoid the checker-board type oscillation. The MUSCL (Monotone Upwind Scheme for Conservation Law) scheme by van Leer[9] was also adopted for the convective term at the region away from the vehicle where the upwind dissipation does not affect the wake and near-wall turbulence of the target vehicle.

The time marching was based on the fractional step method by Kim & Moin[10], in which the third-order Adams-Moulton scheme or the implicit Euler scheme was adopted for the velocity prediction step. The coupling of velocity and pressure field to obtain the pressure and to correct the velocity was based on the SMAC (Simplified Marker and Cell) method by Amsden and Harlow[11]. Flow rate on the control-volume surface was estimated following the method proposed by Rhie and Chow[12] to keep off the checker-board type pressure oscillation. The pressure Poisson equation was solved by the ICCG (Incomplete Cholesky Conjugate Gradient) method.

3.3 Computational Domain and Boundary Conditions

The shape of the computational domain is of a rectangular duct as shown in Fig. 2, which covers 3.14L upstream of the vehicle model, 6.86L downstream, 4.0W on both sides, and a height of 7.2H. At the inlet boundary, the approach flow was set to be constant and uniform at a velocity of 16.7 m/s. The corresponding Reynolds number is 2.3 x 10^5, based on the vehicle model length L. At the outflow boundary, zero gradient condition was imposed. The ground surface was divided into two regions in which free-slip wall boundary was imposed to the 3.0L from the inlet for simulating the suction floor effect which prevent the development of boundary layer, while the remaining ground surface was treated by the wall-model assuming a fully developed turbulent boundary layer. As for the surface of the vehicle model, the log-law distribution of instantaneous velocity was imposed. Finally, the ceiling and lateral boundaries of the domain were treated as free-slip wall boundary.

The computational domain is discretized into around 16 million elements with 5 million nodes. In addition, finer elements are constructed nearby the vehicle model to capture more details of the flow information near the vehicle, in particular, at the pillars and the truck deck regions (see Fig. 3) for the sedan-type vehicle model cases. Fifteen layers of prism mesh are generated from the surface with the thickness of the first layer being 0.1 mm. In the case, the typical wall distance of the first nearest grid point is less than 150 in wall unit (y^+), which is within the logarithmic layer of the mean velocity profile. Three layers of prism mesh are also generated at the outlet boundary while the remaining domain volume is constituted of tetrahedral cells.

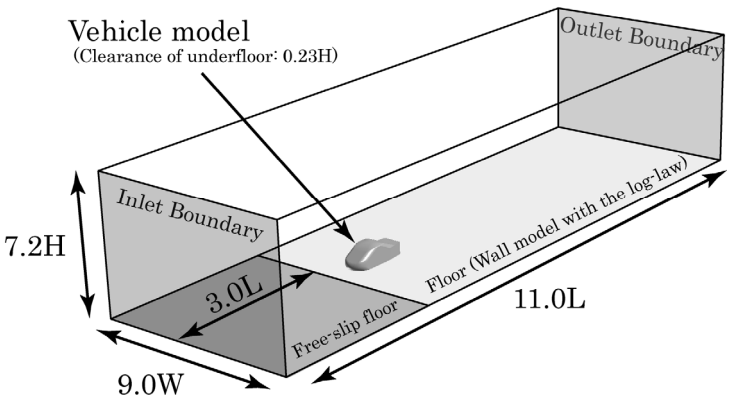

Figure 2: Computational Domain.

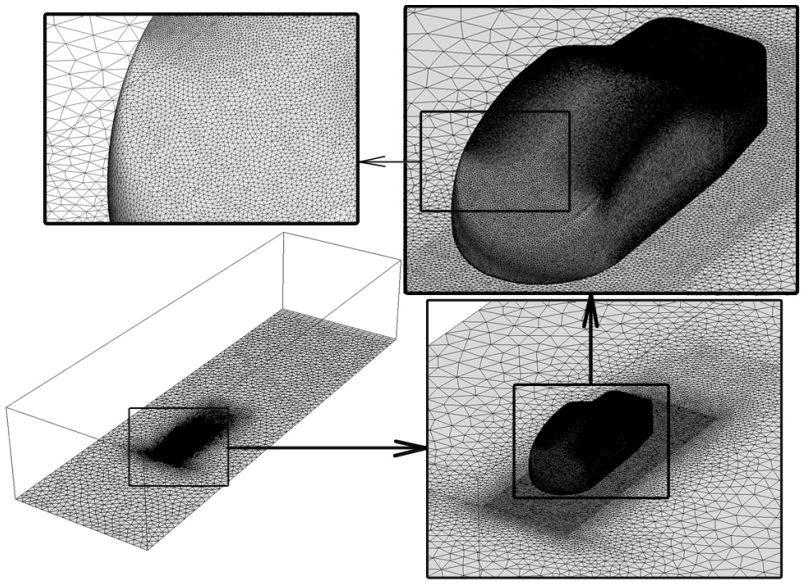

Figure 3: Surface Grid Resolution.

3.4 Pitching Conditions

For the dynamic pitching simulation, a forced-sinusoidal-pitching oscillation is imposed on the vehicle model during LES calculation. This is achieved by employing the Arbitrary Lagrangian-Eulerian (ALE) technique [13]. The axis of rotation is at the underfloor of vehicle model where front wheel axle will be located if in the case of a rear sedan car. This is in accordance to the result of Okada et al [4] where during road

test, fluctuation of rear-ride height is of higher significant compared to front-ride height. Moreover, sedan vehicle of lower pitching stability is having relatively higher rear-ride height fluctuation compare to vehicle of higher pitching stability. Hence, the simplified vehicle models are set into pitching motion in a manner that simulating the rear-ride height fluctuation of the real sedan car during road test. The pitch angle θ is defined as:

$$\theta = \theta_0 + \theta_1 \sin\phi(t), \qquad \phi(t) = 2\pi f t \tag{7}$$

By setting θ_0 and θ_1 equaled to 2, the vehicle models are forced to oscillate between 0° to 4° pitch angle. To minimized grid distortion, the initial grid is created with the vehicle model inclining at 2° pitch. Then, ALE technique is employed to rotate the vehicle model to the maximum pitch of 2° relative to the initial value in the positive and negative directions.

The frequency f is of 10 Hz, which is equivalent to the Strouhal number St of 0.13. This value is chosen considering the road test St of 1.5 by Okada et al [4]. Thus in the present LES study, the vehicle models completed a full phase of oscillation in every 0.1 sec. Phase-averaged results presented in this paper are averaging over 15 phases after the LES computation achieved stable periodic conditions. Conventions of coordinates, pitch angle and moment are as shown in Fig. 4.

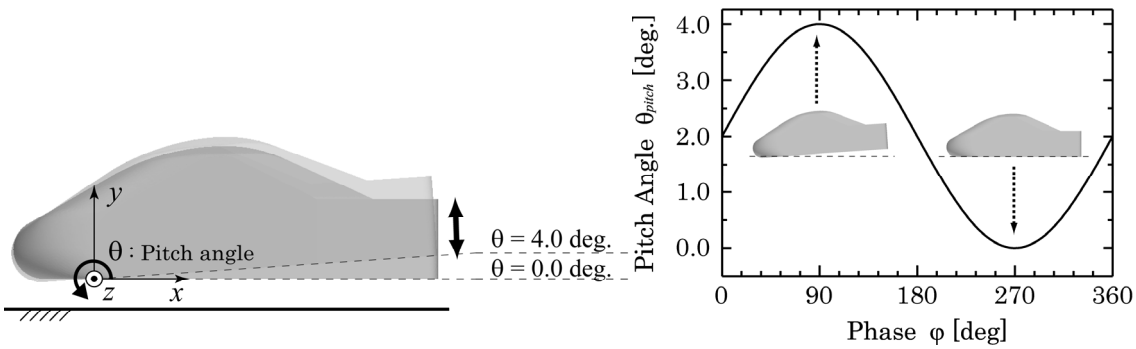

Figure 4: Conventions of coordinates, pitch angle and pitch moment

4 FLOW STRUCTURES ABOVE THE TRUNK DECK

4.1 Static condition

To confirm whether the dominant flow structures supposed in the previous studies are properly captured, LES of flow around the two simplified vehicles at the static pitch angle of 0° were conducted. Fig. 5 shows the ISO-surfaces of time-averaged vorticity magnitude of 1.5 x 10^3 [1/s] (arrows indicate the rotational directions) where front and rear pillar vortex pairs are apparent in model A, while a pair of rear pillar vortex is pertaining to model B-rev without the front pillar vortices.

The separation zone which detached near the trailing edge of the roof is also apparent in model A, whereas attached flow is observed in model B-rev before separation occurred at the rear shield. This is attributed to the used of a more streamline profile near the roof's trailing edge of model B-rev.

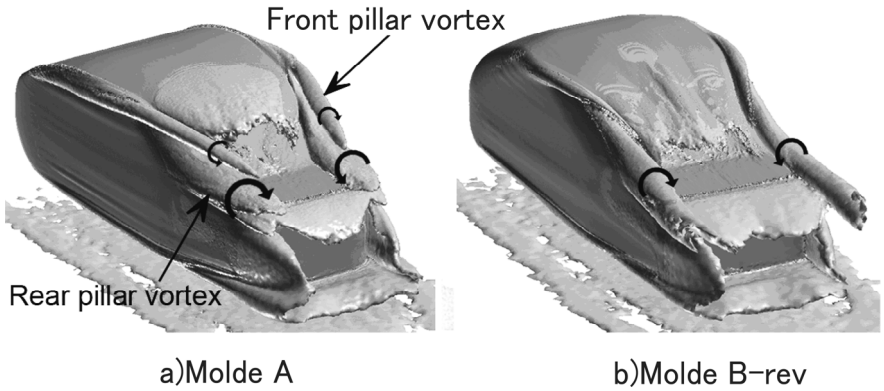

Figure 5: Front and rear pillar vortices.

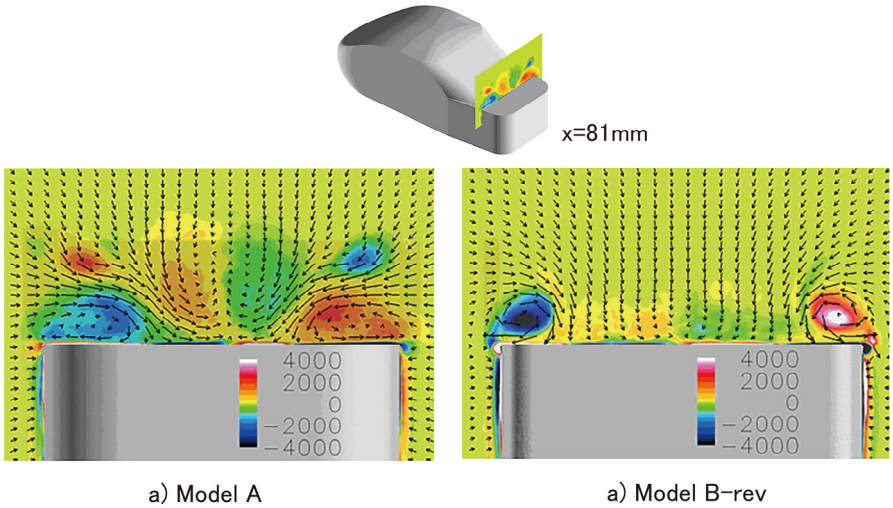

Figure 6: Mean cross-flow velocity distribution and velocity magnitude above the trunk deck.

Figure 6 shows the cross flow velocity distribution above the trunk deck with the front and rear pillar vortices depicted as the time-averaged vorticity magnitude. The size of the rear pillar vortices appears to be inversely proportional to its intensity. In model B-rev where the rear pillar vorticity is higher, the surrounding flow which being drawn inwards into the region above the trunk deck by the rear pillar vortex pair, rotates in a close proximity around the vortex core near the side edges of the trunk deck. Consequently, the flow above the trunk deck appears to be very two-dimensional, i.e. of very weak cross flow components. In model A however, the size of the rear pillar vortices is the largest and least intense. The surrounding flow which being drawn inwards rotates around it, meanwhile some rolled-in flow away from the vortex core crosses towards the centerline of the trunk deck, thus results in a very strong cross flow above the trunk deck surface. Also, there is a pair of front pillar vortex situated above the rear pillar vortex pair which is rotating in an opposite sense. As depicted, the front pillar vortex pair is interacting with the rear pillar vortex pair and enhances the cross flow above the trunk deck. Furthermore, this cross flow which approaches the centerline of the trunk deck from both sides, converges at the centerline and then rolling upwards. As a result, an upwash circulatory flow structure is generated.

4.2 Dynamic condition

The vortical structures emanating from the front and rear pillar that propagated downstream above the trunk deck are also captured in the dynamic sinusoidal pitching condition. Fig. 7 shows the cross flow velocity distribution above the trunk deck with the front and rear pillar vortices. The results are phase-averaged quantities for four phases (i.e. at minimum pitch of 0°, during tail up pitching of 2°, at maximum pitch of 4°, and during tail down pitching of 2°) as the vehicle models undergone dynamic pitching oscillation. Compared to the 0° stationary cases, the vorticity of all the vortices appears weaker in the dynamic conditions, but in general, the same principle applies as for the mechanism of how cross flow above the trunk deck is generated in model A, and the formation of two-dimensional flow in model B-rev.

In addition, some transient behaviors may be detected in the vortical structures of model A. As the vehicle model reaches 4° pitch, the front and rear pillar vortex pair had been brought into a closer contact. These vortices do not merge however, instead, the rear pillar vortices are being squeezed into a triangular shape, while the front pillar vortices shifted a little outwards accompany by a slight increased in its vorticity. At this instant, flow comes from the gap between the two vortices appears to be drawn upwards before it is being diverting downwards and then crosses the trunk deck and develops an upwash circulatory flow structure. Ahmed et al. [14] reported that the strength of side edge vortices is mainly determined by the slant angle of the edges where these vortices are emanated. Hence, the increased of the strength in the front pillar vortex pair may be attributed to the increased of the slant angle of the front pillar edges as the vehicle model reaches its maximum pitch.

Figure 8 shows the static pressure C_p and velocity distribution above the trunk deck, along the centerline of model A and B-rev at various phases. As illustrated, the upwash flow structure above the trunk deck of model A can be evidenced by the up-pointing velocity vector. Besides, the static pressure distribution in this flow region is relatively lower than in model B-rev owning to the strong circulatory flow component. The distinct flow patterns above the trunk deck exhibited in model A and B-rev have strong influence on their pitching stability characteristic, which will be discussed in the following sections.

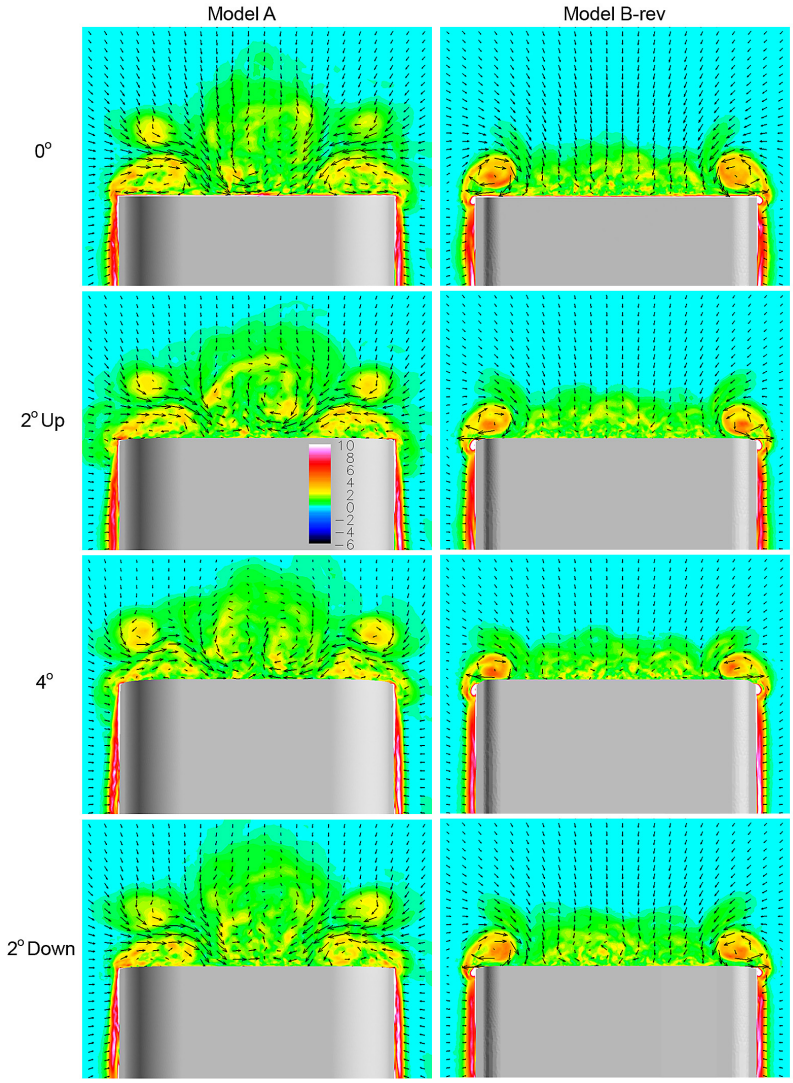

Fig. 7 Phase-averaged cross flow velocity distribution and vorticity magnitude above the trunk deck at various phases; x = 81 mm.

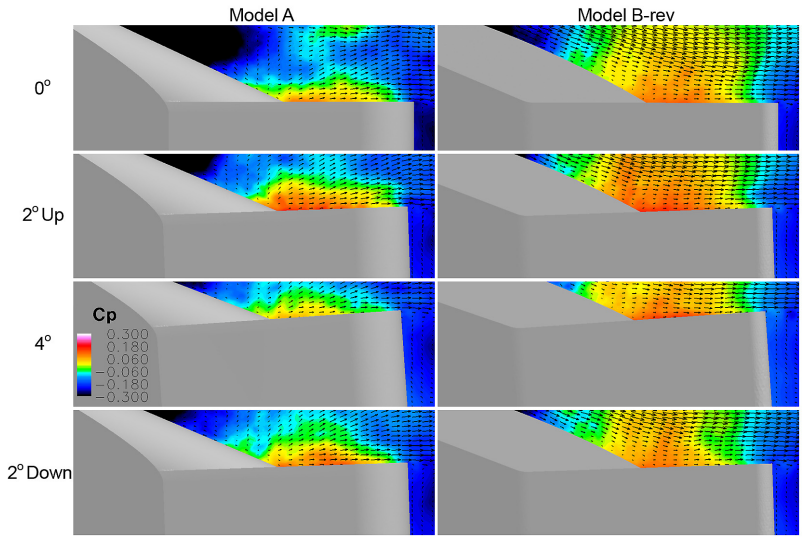

Fig. 8 Phase-averaged static pressure C_p and velocity distribution at various phases along the centerline; model A and B-rev.

5 AERODYNAMIC DAMPING

As the forced pitching oscillation given by eq. (7) as input, the aerodynamic response was measured and averaged over the phase ϕ. The phase-averaged pitching moment obtained is shown in Fig. 9. The pitching moment with respect to the phase is generally sinusoidal with its phase about π/2 ahead of the pitching angle imposed. The moment shows maximum peak during the rear of the vehicle going down, and vice versa. Thus we can say from the figure that both models are aerodynamically stable with regard to the pitching oscillation. However, some difference between the two models is also identified in terms of their phase shifting and peaks.

In order to evaluate more quantitatively their difference concerning the steady and unsteady aerodynamic components against the imposed pitching angle, the phase-averaged pitching moment is decomposed. We can assume the pitching moment acting on the model as following expansion for a variation of pitch angle θ,

$$M = C_0 + C_1\theta + C_2\dot{\theta} + C_3\ddot{\theta} \tag{8}$$

The first coefficient C_0 represents an aerodynamic moment in a stationary state. The C_1 on the second term expresses a quasi-stationary effect which is proportional to the pitch angle. The C_2 on the third is an aerodynamic damping factor of the pitch oscillation if it is negative. In fact, this is the most important factor to determine the aerodynamic pitching stability focusing in this study. The C_3 represents the component proportional to the angular acceleration, which is sometimes called as "additional mass effect". Substituting the sinusoidal pitching motion given by eq. (7) into eq. (8), we can obtain following expression for the pitching moment:

$$M = (C_0 + C_1\theta_0) + \{C_1 - (2\pi f)^2 C_3\}\theta_1 \sin\phi(t) + 2\pi f\theta_1 \cos\phi(t) \tag{9}$$

Then, it can be rewritten by using new coefficients $C_{\sin}$ and $C_{\cos}$ as follows;

$$M = C_{\mathrm{stat}} + C_{\sin}\sin\phi(t) + C_{\cos}\cos\phi(t) \tag{10}$$

Based on the least mean square fitting to the phase-averaged pitching moment shown in Fig. 9, we can obtain the coefficients included in eq. (10). In Fig. 9, the resulting approximated profiles are also plotted for reference. The decomposed components of the approximated profiles are illustrated in Fig. 10, and the three coefficients obtained are summarized in Table 1.

The first component C_{stat} is absent of the influence of phase changed, thus the value may be obtained through stationary approach by setting the vehicle model at 0° pitch. This component sets the baseline of M. Howell and Good [15] and Hucho [16] reported that nose up M is desirable in the context of directional stability at high speed, thus the values obtained for all the vehicle models deem unfavorable for such performances, though model B-rev having a relatively lower value, which is better than model A. Meanwhile, since the displacement of the vehicle models is given in the form of sine function, the second term at the right of eq. (10) that in phase with the displacement does no work upon the models.

Thus, discussion concerning the dynamic response of the models should be based on the third term which makes a π/2 shift in ϕ. Here, the negative value of the third term means it is a component that tends to resist the rotational motion of the model. Hence, it is to be considered as the aerodynamic damping which stabilizes the pitching motion of the vehicle models. As presented in Table 1, model B-rev exhibits higher aerodynamic

damping than model A. This trend is in agreement to our expectation as model B-rev is created based on the sedan-type vehicle of higher pitching stability whereas model A the lower.

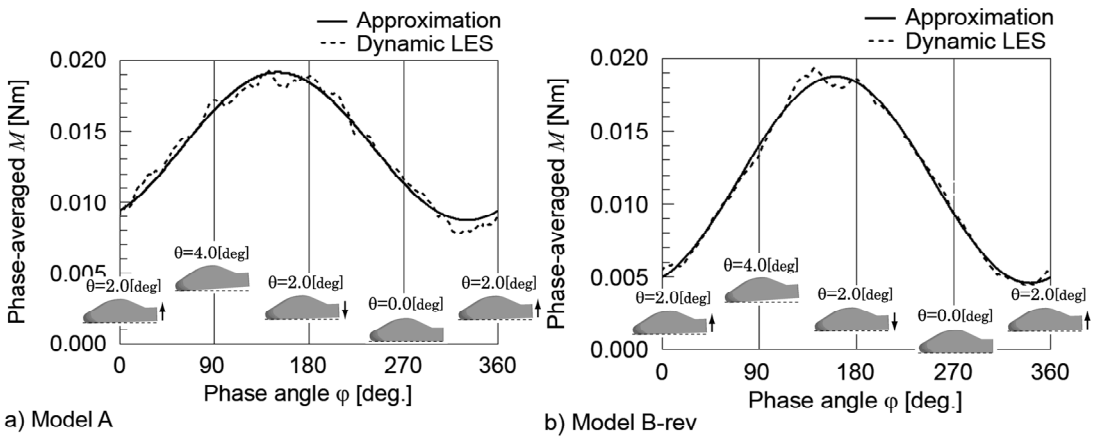

Fig. 9 Phase-averaged pitching moment and their approximations.

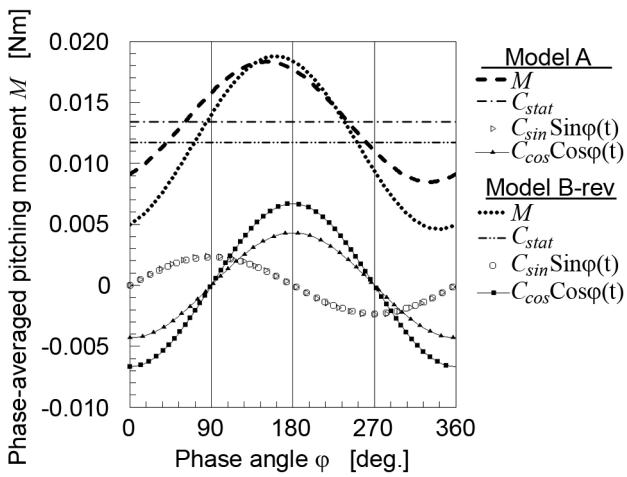

Fig. 10 Decomposition of the phase-averaged pitching moment.

Table 1 Approximation function coefficients of phase-averaged aerodynamic pitch moment

Model	C_{stat}	C_{sin}	C_{cos}
A	1.39×10^{-2}	2.59×10^{-3}	-4.53×10^{-3}
B-rev	1.17×10^{-2}	2.33×10^{-3}	-6.69×10^{-3}

6 CONCLUSIONS

Pitching stability characteristics of sedan-type vehicle were assessed by conducting the LES of flow around the simplified vehicle models subjected to forced-sinusoidal-pitching oscillation. Distinct flow patterns above the trunk deck associated with sedan-type vehicles of different pitching stability characteristics are primarily affected by the front and rear pillar vortex pair. In the case of high intensity rear-pillar vortices (model

A), flow above the central region of the trunk deck is relatively two-dimensional along the streamwise direction, whereas strong cross flow and upwash circulatory flow field is developed in the lower rear-pillar vorticity case (model B-rev). In conjunction with this, it was demonstrated that vehicle model of higher aerodynamic damping is found to be associated with the former, while the lower damping model pertaining to the latter.

ACKNOWLEDGEMENTS

This work has been supported by Industrial Technology Research Grant Program in 2007 from New Energy and Industrial Technology Development Organization (NEDO) of Japan. This study was conducted under the collaboration research projects with Mazda Motor Corporation, and the shape data together with experimental data provided are greatly acknowledged.

REFERENCES

[1] A. Cogotti, Generation of a Controlled Level of Turbulence in the Pininfarina Wind Tunnel for the Measurement of Unsteady Aerodynamics and Aeroacoustics, *SAE Technical Paper* No. 2003-01-0430 (2003)

[2] J. Mayer, M. Schrefl, and R. Demuth, On various Aspects of the Unsteady Aerodynamic Effects on Cars Under Crosswind Conditions, *SAE Technical paper* No.2007-001-1548, (2007)

[3] K. R. Cooper, and S. Watkins, The Unsteady Wind Environment of Road Vehicles, Part One: A Review of the On-road Turbulent Wind Environment, *SAE Technical Paper* No.2007-01-1236 (2007)

[4] Y. Okada et al., Flow structures above the trunk deck of sedan-type vehicles and their influence on high-speed vehicle stability 1st report: On-road and wind-tunnel studies on unsteady flow characteristics that stabilize vehicle behavior, *SAE Int. J. of Passenger Cars – Mechanical Systems*, **vol.2** no.1, pp.138-156 (2009)

[5] T. Nakashima et al., Flow structures above the trunk deck of sedan-type vehicles and their influence on high-speed vehicle stability 2nd report: Numerical investigation on simplified vehicle models using Large-Eddy Simulation, *SAE Int. J. of Passenger Cars – Mechanical Systems*, **vol.2** no.1, pp.157-167 (2009)

[6] M. Tsubokura et al., Development of an unsteady aerodynamic simulator using large-eddy simulation based on high-performance computing technique, *SAE Int. J. of Passenger Cars – Mechanical Systems*, **vol.2** no.1, pp.168-178 (2009)

[7] J. Smagorinsky, General circulation experiments with the primitive equations, I. The Basic Experiment, *Monthly Weather Rev.*, **vol.91**, Num. 3, pp.99-164 (1963)

[8] S. Muzaferija, Adaptive finite volume method for flow predictions using unstructured meshes and multigrid approach, Ph.D thesis, University of London (1994)

[9] B. van Leer, B., Toward the ultimate conservative difference scheme 4, a new approach to numerical convection, *Journal of Computational Physics*, **vol. 23**, pp.276-99 (1977)

[10] J. Kim and P. Moin, 1985, Application of a fractional step method to incompressible Navier-Stokes equations, *Journal of Computational Physics*, **vol. 59**, pp.308-323 (1985)

[11] A. A. Amsden and F. H. Harlow, A simplified MAC technique for incompressible fluid flow calculations, *Journal of Computational Physics*, **vol. 6**, pp.322-325 (1970)

[12] C. M. Rhie and W. L. Chow, A numerical study of the turbulent flow past an isolated airfoil with trailing edge separation, *AIAA Journal*, **vol. 21**, pp.1525-32 (1983)

[13] C. W. Hirt, A. A. Amsden, and J. L. Cook, An Arbitrary Lagrangian-Eulerian Computing Method for All Flow Speeds, *Journal of Computational Physics*, **vol. 14,** pp. 227-253 (1974)

[14] S. R. Ahmed, G. Ramm, G. Faltin, Some salient features of the time-averaged ground vehicle wake, *SAE Technical paper* No.840300 (1984)

[15] J. Howell and G. L. Good, The influence of Aerodynamic Lift on High Speed Stability, *SAE Technical Paper* No. 1999-01-0651 (1999)

[16] W.-H. Hucho, Aerodynamics of Road Vehicles, 4nd ed., *SAE, Inc.*, Warrendale, PA, USA, Chap. 5, 252 (1998)